CRYSTAL GROWTH & DESIGN

Article

pubs.acs.org/crystal

Nucleation Studies of Active Pharmaceutical Ingredients in an Air-Segmented Microfluidic Drop-Based Crystallizer

Jennifer Lu,[†] James D. Litster,*[,†,‡] and Zoltan K. Nagy[†]

[†]School of Chemical Engineering and [‡]School of Industrial and Physical Pharmacy, Purdue University, West Lafayette, Indiana 47907, United States

ABSTRACT: In this work, an innovative experimental platform to study the nucleation behavior of an active pharmaceutical ingredient (API) using a gas-segmented flow produced by a microfluidic T-junction device with fine perfluoroalkoxy alkane (PFA) tubing is presented. In the experiments, a continuous airflow was used to segment the supersaturated liquid phase into nearly monodispersed droplets (with a coefficient of variance about 15% of the drop size distribution) at the T-junction. As the API molecules have relatively low gas/solvent partition coefficients, mass transfer between phases is effectively inhibited. Nucleation then occurred within the drops in the temperature-controlled capillary crystallizer. By treating the probability of crystal nucleation in each drop as a nonstationary Poisson process, the effect of process conditions on lactose and aspirin nucleation was studied. In lactose nucleation studies, the Poisson rate process effectively captures the nucleation behavior, and the estimated nucleation parameters show good agreement to literature values. However, the lactose nucleation rate increased more sharply with a supersaturation ratio than predicted by classical nucleation theory. The validation of aspirin nucleation studies from ethanol demonstrates the application of this newly design system for crystallization of relatively nonpolar organic molecules from nonaqueous solvents to give crystals with controlled attributes.

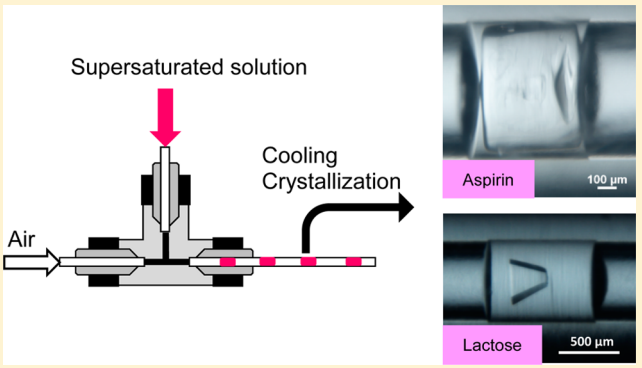

INTRODUCTION

Crystallization is a widely employed unit operation in different manufacturing industries. It is a process in which a highly ordered solid phase forms from a solution or melt and has been widely used as a method of separation and purification. Despite its importance, crystallization still remains one of the least understood and most complicated processes to control because of our inability to monitor and control primary nucleation, which strongly dictates the characteristics of the crystal product. For example, in active pharmaceutical ingredient (API) manufacture, tight control of crystal attributes is needed as they strongly affect the downstream processing of the solid dosage form and ultimately the bioavailability of the drug.[1] Therefore, the primary bottleneck to the operation of production-scale drug manufacturing facilities is often associated with difficulties in controlling the size distribution of crystals.[2] New methodologies and systems are needed to serve as a better platform for fundamental crystallization studies and to enable controlled size API production.

The overall crystallization process consists of at least two major events, nucleation and crystal growth. Nucleation, in particular, is a stochastic phenomenon that remains poorly understood and difficult to control in traditional industrial batch crystallizers. Primary nucleation refers to the formation of a crystal from systems that do not contain crystalline matter. In the past century, classical nucleation theory (CNT) has provided a generally accepted concept for primary nucleation, in which the nuclei formation process is seen as a series of molecules attachment to the crystal cluster. The formation of new interfaces accompanied by the growth of cluster size results in an increase in free energy, while the formation of solid from supersaturated solution decreases the free energy. Once the system overcomes the free energy barrier resulting from this competition by reaching a critical cluster size, nucleation occurs.[3] Recently, the concept of CNT has been questioned by the increasing number of studies related to prenucleation clusters[4,5] and the two-step mechanism.[6−8] While the CNT fails to provide an adequate description of all nucleation processes, there is still a lack of a definitive data set to support establishing the multistage nucleation theory. A much better experimental platform is needed to study nucleation under highly controlled and reproducible conditions in order to develop and validate predictive models.

Conventional batch crystallization has high process variability from batch to batch often due to variation in nucleation rates. Continuous processes offer a more efficient and streamlined approach. However, the introduction of residence time distribution within a conventional continuous mixed tank system leads to a broader product size distribution. Emulsion-based particle production has been commonly used in

Received: February 2, 2015
Revised: May 27, 2015
Published: June 16, 2015

DOI: 10.1021/acs.cgd.5b00150
Cryst. Growth Des. 2015, 15, 3645−3651

controlled size polymeric colloidal and inorganic particle production with excellent results.[9,10] This method produces particles of narrow size distribution, and the particle size is controlled by the number of nuclei followed by nearly uniform growth of particles. Using similar concepts, crystallization in emulsions[11,12] did not produce as narrow size distributions as emulsion-based polymerization due to the more complex nature of crystallization. Allen et al. found that polycrystalline particles with a similar size were produced within a certain range of microemulsion drop sizes.[11] Though no statistical analysis was reported, the study supported the idea of using these confined drops as individual crystallizers.

The proof-of-concept of surfactant-free microfluidic drop-based crystallizers to produce very narrow crystal size distributions has been demonstrated with lactose and lysozyme.[13,14] Dombrowski et al.[13] proposed a process where a continuous organic fluid flow was brought into the T-junction microfluidic device to segment the aqueous mother liquor into monodisperse droplets followed by cooling crystallization within different diameter tubing. Their results showed narrow droplet size distributions. The coefficients of variation, representative of the spread of the size distribution, for all tubing systems was less than 2.5%, indicating that the T-junction produced effectively monosized drops. Lactose, known as a material with growth rate dispersion, and lysozyme were crystallized. The product lactose crystal size distribution was narrow, with a 7% coefficient of variation. The drop-based crystallizer in which one crystal is formed per drop imposes a limiting boundary on the maximum size of the grown crystal, thus diminishing the effects of growth rate dispersion on broadening the crystal size distribution.

This platform is ideally suited to nucleation studies because of the highly reproducible mixing and cooling profile in each drop crystallizer, and the capillary crystallizer provides good environmental control to form uniform crystal morphology. Recently, different drop-based microfluidic systems with improving solvent compatibility compared to classic poly(dimethylsiloxane) devices have been developed for kinetic studies of organic molecules crystallization.[15,16] However, drop size evolution and solute concentration change due to mass transfer were observed in system with partially miscible fluids.[16] Moreover, typical small molecule APIs are less polar and more soluble in some organic solvents, leading to the partitioning of solute from the drop phase to the carrier phase. In these cases, estimated crystallization kinetics will deviate from the real natures with overestimated solute supersaturation levels. Therefore, a better platform and better dispersed/carrier fluid combinations are needed.

Recently, there has been interest in using gas as the carrier phase within multiphase systems. There will be less partitioning of solute into the carrier phase compared to liquid−liquid two phase systems. Eder at al. demonstrated using a segmented gas-slurry flow to generate acetylsalicylic acid crystals with relatively narrow size distribution due to narrower residence time.[17] Air-segmented flow shows good mixing condition within the segmented liquid slugs due to recirculation motion in the liquid layer.[18,19] Jiang et al. demonstrated a continuous air-segmented slug-flow crystallizer design that show potential control over crystal properties.[19] This system had a relatively large tube diameter (3.1 mm ID), and hundreds of crystals are produced in each liquid slug.

In this paper, an innovative method to produce controlled-size lactose and API crystals using air as the carrier fluid in microfluidics is implemented. As the API molecules have relatively low gas/solvent partition coefficients, mass transfer and depletion of supersaturation can then be effectively inhibited. Because of the stochastic nature of nucleation, the nucleation rate can be derived from experiment by treating the probability of crystal nucleation in each drop as a nonstationary Poisson process. In this study, results for crystallization of lactose, ibuprofen, and aspirin as the model organic molecules are presented. The ability of the new device to produce API crystals is evaluated, and nucleation studies for the model compounds are presented.

THEORY

Solute Partitioning in Oil- and Air-Segmented Microfluidic Drops. Typical small molecule APIs are less polar and more soluble in specific organic solvents, leading to the possibility of transferring too much solute from the drop to the carrier fluid. This partition effect can be explained by estimating the theoretical partition coefficient for each component in the system. At equilibrium the partition of molecule i between two phases can be defined with the partition coefficient $PC_i^{\nu(2,1)sat}$, the ratio of activity coefficients of molecule i in each phase:[20,21]

$$PC_i^{\nu(2,1)sat} = \frac{\gamma_i^{\nu(1)sat}}{\gamma_i^{\nu(2)sat}} = \frac{X_i^{\nu(2)sat}}{X_i^{\nu(1)sat}} \quad (1)$$

where $\gamma_i^{\nu(k)sat}$ is the activity coefficient of molecule i in phase k, and $X_i^{\nu(k)sat}$ is the mole fraction of molecule i in phase k. By considering the intermolecular forces of attraction that must be overcome in removing a molecule from the solid phase and depositing it in the solvent, the activity coefficient of molecule i can be rewritten in terms of the solubility parameters δ_k,[21] and eq 1 becomes

$$\ln PC_i^{\nu(2,1)sat} = \frac{[(\delta_i - \delta_{\nu(1)})^2 - (\delta_i - \delta_{\nu(2)})^2]V_i}{RT} \quad (2)$$

where V_i is the molar volume of molecule i, R is the ideal gas constant, and T is the absolute temperature.

Consider forming saturated ethanol solution droplets of ibuprofen (2-(4-isobutyl-phenyl)-propionic acid) in silicon oil. The solubility parameters for ibuprofen,[22] ethanol,[23] and silicone oil[24] are 20.9 $MPa^{1/2}$, 26.2 $MPa^{1/2}$, and 16.36 $MPa^{1/2}$, respectively. The molar volume of ibuprofen is 195.5 $cm^3\ mol^{-1}$.[21] Substituting into eq 2 gives the partition coefficient of ibuprofen between ethanol (phase 1) and silicone oil (phase 2) at 25 °C:

$$PC_{ibuprofen}^{\nu(2,1)sat} = 1.80 = \frac{X_{ibuprofen}^{\nu(2)sat}}{X_{ibuprofen}^{\nu(1)sat}} \quad (3)$$

That is, there will be a significant amount of ibuprofen partitioning into silicon oil at equilibrium, which strongly inhibits nucleation due to the depletion of supersaturation.

On the other hand, the partition to gas is related to the vapor pressure of ibuprofen. At room temperature (25 °C), pure ibuprofen exerts a negligible vapor pressure ($P^{\circ}_{ibuprofen} = 6.32 \times 10^{-3}$ Pa).[25] The solubility of ibuprofen in ethanol solution $C_{ibuprofen-sat}$ is 2.2882 M, and the molar fraction of ibuprofen in saturated ethanol solution $X_{ibuprofen-l}$ is 0.207.[26] Treating the saturated ibuprofen−ethanol droplet as ideal solution, the gas phase as ideal gas, and assuming equal volume of the liquid and

DOI: 10.1021/acs.cgd.5b00150
Cryst. Growth Des. 2015, 15, 3645−3651

gas phase, the fraction of the partitioned ibuprofen can be estimated with Raoult's law and the ideal gas law:

$$\frac{N_{\text{ibuprofen-g}}}{N_{\text{ibuprofen-l}}} = \frac{P_{\text{ibuprofen}}V_g}{RT} \times \frac{1}{N_{\text{ibuprofen-l}}} = \frac{P_{\text{ibuprofen}}}{RT} \times \frac{V_l}{N_{\text{ibuprofen-l}}}$$

$$= \frac{P^{\circ}_{\text{ibuprofen}}X_{\text{ibuprofen-l}}}{RT} \times C_{\text{ibuprofen-sat}} = 1.21 \times 10^{-6} \quad (4)$$

where $N_{\text{ibuprofen-g}}$ and $N_{\text{ibuprofen-l}}$ are the moles of ibuprofen in the gas and liquid phase, respectively. $P_{\text{ibuprofen}}$ is the vapor pressure of ibuprofen, R is the ideal gas constant, T = 298.15 K is the absolute room temperature, and V_g, V_l are the volume of the gas and liquid phase, respectively. Thus, the partition effect in the liquid−gas system is negligible, and introducing gas as the carrier phase is an effective way to inhibit supersaturation depletion during crystallization process.

Primary Nucleation Kinetics. Because of its stochastic nature, primary nucleation can be regarded as a random event. By assuming the formation of each nucleus is an independent event, a homogeneous Poisson rate process can account for the random nucleation.[27] The basic concepts were as described by Dombrowski et al.[13] With no crystals present initially, N_0, the number of drops that that do not contain a crystal after time t is

$$N_0(t) = N_t \exp(-J\bar{V}t) \quad (5)$$

where N_t is the total number of drops, J is the nucleation rate, and $\bar{V}$ is the average volume of drops containing supersaturation solution. The primary nucleation rate can be estimated using $P_0(t)$, the probability of forming no nuclei after time t, with the equation:

$$\ln P_0(t) = \ln \frac{N_0(t)}{N_t} = -J\bar{V}t \quad (6)$$

Classical nucleation theory[28] predicts the nucleation rate J as a function of temperature and supersaturation as

$$J = A \exp\left(\frac{-16\pi\gamma^3 V_m^2}{3k^3T^3(\ln S)^2}\right) \quad (7)$$

where γ is the interfacial tension between the crystal and supersaturated solution, V_m is the molecular volume of the crystallized compound, k is the Boltzmann's constant, T is the absolute temperature, and S is the relative supersaturation ratio:

$$S = \frac{C}{C_s} \quad (8)$$

where C is the actual concentration and C_s is the equilibrium saturation concentration at the specific temperature. The kinetic factor A is fit to an Arrhenius dependence:

$$A(T) = A_0 \exp\left(\frac{-E_A}{RT}\right) \quad (9)$$

where A_0 is an Arrhenius nucleation rate pre-exponential factor, E_A is the activation energy associated with molecular attachment to the nucleus, which can include partial loss of the solvent shell or configurational change upon lattice incorporation,[8] and R is the ideal gas constant.

EXPERIMENTAL SECTION

Microdroplet Production. To limit the depletion of supersaturation caused by mass transfer between phases, we propose a new approach using air as the carrier phase to segment the supersaturated solution into monodispersed drops at the microfluidic T-junction. As APIs have low gas/solvent partition coefficients, mass transfer from the drop phase to the carrier phase can be effectively inhibited. A microfluidic T-junction system was assembled and tested to produce air-segmented droplets. Figure 1 shows details of the experimental apparatus. The whole experimental process is divided into three parts: microdroplet production, maturation, and observation. High precision syringe pumps (KD Scientific, Holliston, MA, USA) are used to control the flow rate of both the continuous air flow and the dispersed supersaturated solution into a PEEK microtee assembly (Upchurch Scientific, Oak Harbor, WA, USA) to produce monodispersed microdroplets in PFA tubing. The supersaturated solutions were maintained at elevated temperature during drop production with an infrared lamp to prevent crystallization. The internal diameters of the inlet and outlet PFA tubing (Upchurch Scientific, Oak Harbor, WA, USA) are 150 and 650 μm, respectively. The outlet PFA tubing was 6 m long so that between 50 and 200 drops could be held in the tubing at one time for maturation. The gas flow rate is 500 μL/min, and the supersaturated solution flow rate is 10 μL/min.

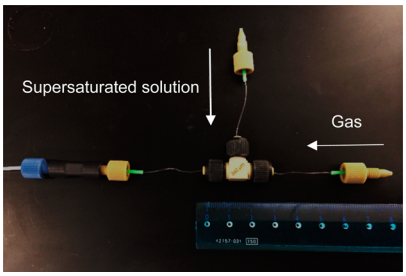

Figure 1. Photograph of the microfluidic apparatus.

Crystallization Solutions Preparation. Lactose, a common pharmaceutical excipient, was chosen for nucleation studies to validate the application of the new platform. Lactose powder (alpha-lactose monohydrate) was obtained from Eli Lilly (IN, USA) to prepare the supersaturated solution for the crystallization studies. Solutions were prepared by dissolving the desired amount of lactose powder in filtered distilled water at 80 °C. The equilibrium saturation concentrations (g/100 g of H_2O) were calculated from the equation as a function of the absolute temperature T:[29]

$$C_{s,\text{lactose}} = \exp(2.398 + 0.028(T - 273.15)) \quad (10)$$

For API crystallization experiments, aspirin (acetylsalicylic acid, >99.0%) and ibuprofen (>98.0%) were both obtained from Sigma-Aldrich (MO, USA). Solutions were prepared by dissolving the desired amount of the compound in filtered distilled ethanol at 75 °C. The equilibrium saturation concentration of aspirin at 25 °C in ethanol is 237.9 g/kg of solvent,[30] and the equilibrium saturation concentrations of ibuprofen (g/100 g of ethanol) were calculated from the following equation as a function of the absolute temperature T:[31]

$$C_{s,\text{ibuprofen}} = 0.497 + 0.001026(T - 273.15)^2 \quad (11)$$

Maturation and Observation. The crystallization experiments were carried out batch-wise using the microfluidic T-junction and PFA tubing. All experiments were conducted by first running the droplet production system for 10 min to reach the steady state. Once the entire length of the tubing was filled with drops (on average 65 drops per experiment), the flows were stopped. The ends of the tubing were carefully sealed, and then the tubing was stored in a temperature controlled water bath. Supersaturation was achieved by cooling the system with the water bath to desired crystallization temperature. Droplets were observed and imaged directly through the transparent

DOI: 10.1021/acs.cgd.5b00150
Cryst. Growth Des. 2015, 15, 3645−3651

PFA tubing with a Nikon SMZ1500 stereomicroscope (Nikon, Tokyo, Japan) and camera at regular intervals of time for the dynamic experiment, and after 24 h for the nucleation studies.

Nucleation Parameters Estimation. Combining eqs 6, 7, and 9 gives the change in fraction of empty drops as a function of supersaturation S and temperature T:

$$P_0(t) = \exp\left(-A_0 \exp\left(\frac{-E_a}{RT}\right) \exp\left(\frac{-16\pi\gamma^3 V_m^2}{3(kT)^3(\ln S)^2}\right)\bar{V}t\right) \quad (12)$$

In the lactose nucleation study, multiple linear regression is implemented to fit the kinetic parameters with data under 20, 30, and 40 °C maturation conditions. The nucleation rate fits were found using the LINEST function in Excel. To use LINEST, eq 12 is linearized to yield the linearized functional form:

$$\ln\left(-\frac{\ln(P_0(t))}{\bar{V}t}\right) = \ln(A_0) - \frac{E_a}{RT} - \frac{16\pi\gamma^3 V_m^2}{3k^3T^3\ln(S)^2} \quad (13)$$

Equation 13 is the basis for the multiple regression fit of the form:

$$y = m_1x_1 + m_2x_2 + b \quad (14)$$

$$y = \ln\left(-\frac{\ln(P_0(t))}{\bar{V}t}\right),\ x_1 = \frac{1}{T},\ x_2 = \frac{1}{T^3\ln(S)^2} \quad (15)$$

$$m_1 = -\frac{E_a}{R},\ m_2 = -\frac{16\pi\gamma^3 V_m^2}{3k^3},\ b = \ln(A_0) \quad (16)$$

For aspirin nucleation studies, simple linear regression, similar to the above procedure but considering kinetic factor A as a constant, is implemented to fit the kinetic parameters as the following equations:

$$y = mx + b \quad (17)$$

$$y = \ln\left(-\frac{\ln(P_0(t))}{\bar{V}t}\right),\ x = \frac{1}{\ln(S)^2} \quad (18)$$

$$m = -\frac{16\pi\gamma^3 V_m^2}{3k^3T^3},\ b = \ln(A) \quad (19)$$

RESULTS AND DISCUSSION

Air-Segmented Microdroplets Production System. Perfluoroalkoxy alkane (PFA), with low coefficient of friction and permeability, high temperature stability, and chemical resistance (virtually identical to polytetrafluoroethylene), serves as an ideal material for the tubular crystallizer. Also, the relatively low surface energy and large contact angle give advantages forming liquid droplets in a continuous gas flow. The sample drop size distribution produced in the 650 μm PFA tubing with an aqueous phase flow of 10 μL/min and a gas phase flow rate of 500 μL/min is shown in Figure 2. The size distribution was measured as number-based distribution with the drop size defined as the volume equivalent diameter. The coefficient of variance CV, defined as the ratio of the standard deviation to the mean, was used to represent the spread of the drop size distribution. In this example, the mean drop size is 711 μm and the CV is 13%. While this CV is acceptable, the produced drop size distribution is broader than typical aqueous/oil two-phase microfluidic drop based systems in the literature where the CV is approximately 3%.[13,32,33] This is due to the different breakup mechanism in the air−liquid system, and possibly the larger interfacial tension between the liquid and air phases and the high compressibility of air.[34] Recently, Jiang et al.[35] demonstrated a capillary coflow device, with the inner flow of liquid being periodically dispersed into uniform droplets by the coaxial flow of gas. The droplet size and

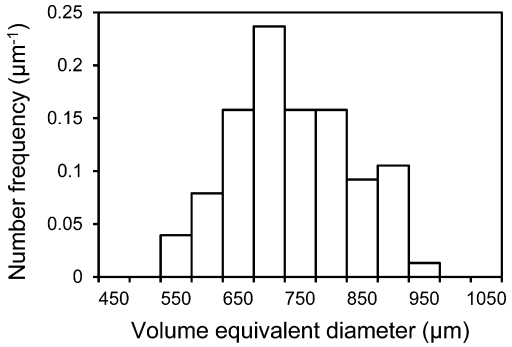

Figure 2. Number-based sample drop size distribution produced from the microfluidic T-junction within the 650 μm ID PFA tubing with an aqueous phase flow rate of 10 μL/min and a gas phase flow rate of 500 μL/min.

different formation modes could be tuned by varying the liquid and gas flow rates. By implementing a similar technique, improved control over the produced droplet size is expected in the future. Mean drop sizes were used in nucleation modeling in the later sections.

Lactose Nucleation Studies. Because of the slow growth rate of lactose, primary nucleation can be modeled as a homogeneous Poisson rate process.[13] The Poisson rate process was tested by measuring the fraction of drops containing zero lactose crystals at different time points at constant temperature with a total droplet amount of 178 over 24 h. If primary nucleation does follow a Poisson rate process, the natural logarithm of the fraction of drops containing no lactose crystal over time should be a linear function of time [eq 6].

Figure 3 shows the fractions of drops containing no lactose crystal over time with the initial supersaturation ratio S = 2.57

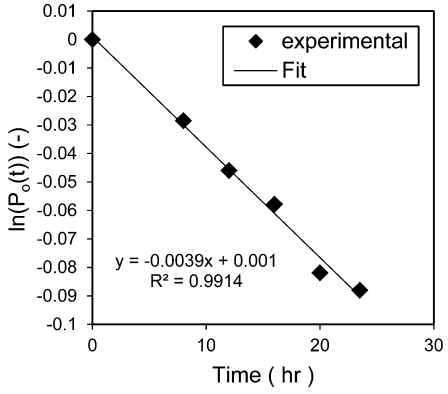

Figure 3. Plot of the nature logarithm of the fractions of uncrystallized to crystallized drops versus time.

at 25 °C. The experimental data fit on a straight line, indicating statistical nucleation according to eq 5. The nucleation rate can be obtained by dividing the slope of the linear fitting curve with the average droplet size. This behavior is consistent with the similar nucleation results for protein and organic compounds from aqueous solution in drop based crystallizers.[36,37] Crystals can only be detected after grown into a certain size, which leads to time delay t_g. Thus, eq 6 is reformulated as

$$\ln P_0(t) = -J\bar{V}(t - t_g) = -J\bar{V}t + J\bar{V}t_g \quad (20)$$

This is observed in Figure 3, in which the nonzero intercept accounts for the delay response. Figure 4 shows the example of

DOI: 10.1021/acs.cgd.5b00150
Cryst. Growth Des. 2015, 15, 3645−3651

a drop containing single crystal with clear Tomahawk morphology.

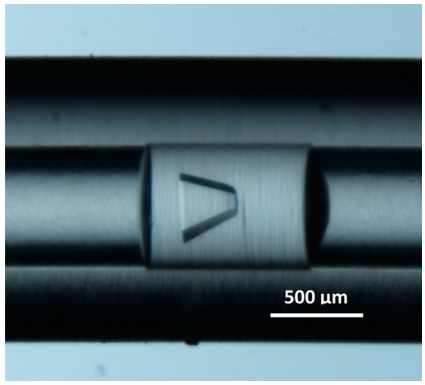

Figure 4. Example of a drop containing single lactose crystal within the 650 μm ID PFA crystallizer.

The effect of temperature and initial supersaturation on lactose primary nucleation was investigated by measuring the fractions of droplets containing no crystals after 24 h at 20, 30, and 40 °C, respectively. Figure 5 shows that the fraction of

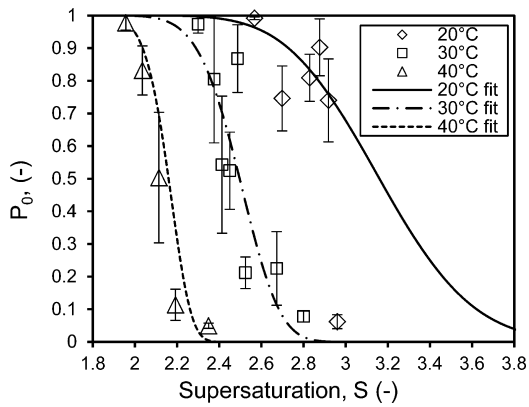

Figure 5. Fraction of drops containing zero lactose crystal after 24 h at 20, 30, and 40 °C, respectively. Each data point is the average of at least three experiments.

droplets containing no crystals after 24 h (P_0) decreases with increasing initial supersaturation ratio S at all temperatures. With eq 6, nucleation rate J was determined and plotted as a function of supersaturation ratio S and temperature in Figure 6. Both figures show that nucleation happens at a lower supersaturation ratio S as temperature increases, and the fraction of droplets containing no crystals at constant supersaturation ratio S decreases with increasing temperature. This is consistent with the classical nucleation theory, in which increases in temperature or supersaturation are expected to produce an increased nucleation rate (see eq 7). At 20 and 30 °C, the experimental change in nucleation rate with increasing supersaturation ratio S is somewhat sharper than predicted by the homogeneous nucleation theory; e.g., note that at T = 20 °C, S = 2.96 the experimental value of P_0 is 0.06 ± 0.02 compared to 0.75 predicted by the homogeneous nucleation theory. One possible explanation of the discrepancy is that some crystals formed in droplets were due to heterogeneous nucleation instead of the homogeneous nucleation described by the classical nucleation theory.

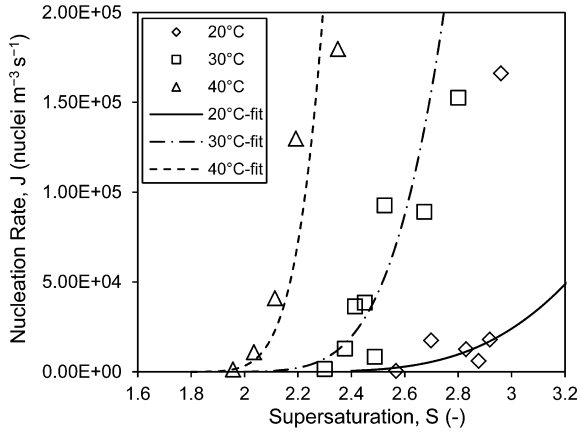

Figure 6. Nucleation rate as a function of supersaturation ratio at 20, 30, and 40 °C, respectively. Each data point is the average of at least three experiments.

Multiple linear regression was used to find the best fit value for the nucleation parameters γ, E_A, and A_0 using the experimentally measured fractions of droplets containing no crystals after 24 h at the three different temperatures. The fitting results are shown in Table 1. The estimated interfacial tension γ and activation energy E_A of lactose nucleation are comparable to the literature value using the aqueous/oil two-phase system[13] despite the broader drop size distribution. Combining A_0 and E_A in eq 9, the estimated value of A is of the order 10^{21} nuclei·m^{-3}·s^{-1}, which is much higher than the literature value with the liquid−liquid system (of the order 10^8 nuclei·m^{-3}·s^{-1}).[13] Possible explanation for the difference in A is that the produced drop volumes are about 5 times larger than ones in prior studies.[13] Heterogeneous nucleation could also take place, leading to higher nucleation rates. By decreasing variation in the produced drop size with an improved device, the air-segmented two-phase system is expected to enable more accurate crystallization kinetics estimation.

Active Pharmaceutical Ingredient (API) Nucleation Studies. To validate API crystallization with the new experimental setup, ibuprofen and aspirin were used as the model APIs and crystallized within pure ethanol solvent. Pure ethanol droplets were first carefully sealed within the PFA tube for 6 days, and the size of the droplets were measured each day. There was no significant difference (t test with $P < 0.05$) of the mean drop size after 6 days. Thus, evaporation of ethanol can be neglected. On the other hand, solvent transfer through the air segment between drops could possibly affect nucleation for volatile solvents. From Raoult's law, the change in ethanol concentration due to the decrease in API concentration in the droplet due to nucleation and crystal growth could lead to change in vapor pressure, causing solvent transfer for volatile solvent like ethanol from a drop containing a crystal to an adjacent drop yet to nucleate. If the solvent transfer is significant, we would expect suppressed nucleation overall due to the ethanol transferring to the noncrystallized droplet thus reducing the supersaturation level. However, we did not observe a measurable change in the drop size over time and so conclude this effect can be neglected at least in this case study. As shown in Figure 7a, with an initial supersaturation S = 3 at 10 °C, ibuprofen crystals were observed after 3 days. Figure 7b shows the aspirin crystal observed after 24 h with an initial supersaturation ratio S = 4.5 at 25 °C. The success of obtaining API crystals within the microfluidic crystallizer ensures the

DOI: 10.1021/acs.cgd.5b00150
Cryst. Growth Des. 2015, 15, 3645−3651

Table 1. Estimated Kinetic Parameters Fitted with CNT for Lactose and Aspirin Nucleation in the Microfluidic Drop-Based Crystallizer

	lactose		Dombrowski et al., 2007[13]	
parameter	best-fit	95% confidence interval	best-fit	95% confidence interval
γ (mN m^{-1})	5.92	5.11/6.56	5.9	5.4/6.3
E_A (kJ·mol^{-1})	190	116/264	110	52/160
A_0 (#m^{-3} s^{-1})	1.20×10^{41}	1.49×10^{27}/ 9.70×10^{54}	5.4×10^{27}	3.7×10^{17}/ 8.0×10^{37}
R^2	0.70		0.72	
	aspirin			
parameter	best-fit	95% confidence interval		
γ (mN m^{-1})	9.54	7.06/11.14		
A (#m^{-3} s^{-1})	1.32×10^{6}	7.43×10^{4}/2.34×10^{7}		
R^2	0.58			

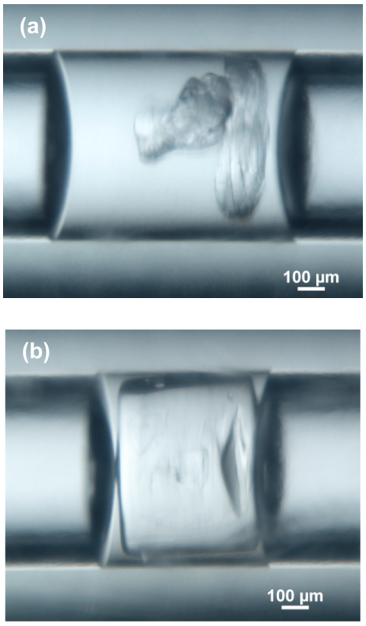

Figure 7. Examples of drops containing crystals of (a) ibuprofen and (b) aspirin in a 650 μm ID PFA crystallizer.

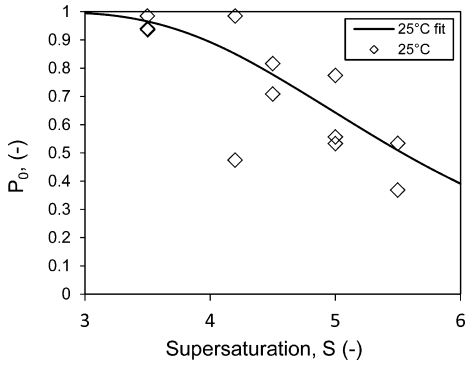

Figure 8. Fraction of drops containing zero aspirin crystal after 24 h at 25 °C.

possibility of studying nucleation and crystal growth of active pharmaceutical ingredients with the proposed method.

A primary nucleation study with aspirin was undertaken to demonstrate the new air segmented system was valid for studying APIs and other small organic molecules. Assuming nucleation follows the homogeneous Poisson rate process, the effect of initial supersaturation on aspirin primary nucleation was investigated by measuring the fractions of droplets containing no crystals after 24 h at 25 °C. Figure 8 shows that aspirin nucleation took place at a higher supersaturation ratio and over a broader range of supersaturations than for lactose nucleation. The experimental data followed the fitted sigmoidal curve with CNT [eq 12]. Linear regression, similar as the lactose nucleation study, was used to find the best fit value for the nucleation parameters γ and A using the experimentally measured fraction of droplets containing no crystals after 24 h. The fitting results are shown in Table 1. The interfacial tension of 9.54 mN m^{-1} is close to value calculated from experimental aspirin nucleation studies (6.79 mN m^{-1})[38] and modeling results (3.65−11.31 mN m^{-1}) for different aspirin nucleation cluster faces.[39]

■ CONCLUSIONS

An innovative air-segmented microfluidic drop-based platform for studying crystallization of organic compounds from aqueous and organic solvents is demonstrated in this paper. Introducing gas as the carrier phase to the drop-based crystallizer effectively inhibits partitioning of the solute between phases and thus enables crystallization of a wide range of organic molecules to be studied. In lactose nucleation studies, the Poisson rate process effectively captures the nucleation behavior, and the estimated nucleation parameters show good agreement to literature values. However, the classical nucleation theory does not fully capture the effect of supersaturation on the measured nucleation kinetics. Aspirin nucleation kinetics from ethanol were successfully measured, demonstrating the application of this newly design system to API crystallization from organic solvents. By decreasing variation in the produced drop size using a coflow device, more accurate crystallization kinetics is expected, and monosize product crystals are possible by achieving nucleation of a single crystal in each drop.

■ AUTHOR INFORMATION

Corresponding Author

*Address: School of Chemical Engineering, Forney Hall of Chemical Engineering, 480 Stadium Mall Drive, West Lafayette, IN 47907-2100. Telephone: +1-765-496-2836. Fax: +1-765-494-0805. E-mail: jlitster@purdue.edu.

Notes

The authors declare no competing financial interest.

DOI: 10.1021/acs.cgd.5b00150
Cryst. Growth Des. 2015, 15, 3645−3651

REFERENCES

(1) Singhal, D.; Curatolo, W. *Adv. Drug Delivery Rev.* **2004**, *56*, 335−347.
(2) Braatz, R. D. *Annu. Rev. Control.* **2002**, *26*, 87−99.
(3) Mullin, J. W. *Crystallization*; Butterworth-Heinemann: Oxford, 2001; Chapter 5, pp 182−189.
(4) Gebauer, D.; Cölfen, H. *Nano Today* **2011**, *6*, 564−584.
(5) Gebauer, D.; Völkel, A.; Cölfen, H. *Science* **2008**, *322*, 1819−1822.
(6) Erdemir, D.; Lee, A. Y.; Myerson, A. S. *Acc. Chem. Res.* **2009**, *42*, 621−629.
(7) Chakraborty, D.; Patey, G. N. *Chem. Phys. Lett.* **2013**, *587*, 25−29.
(8) Davey, R. J.; Schroeder, S. L.; ter Horst, J. H. *Angew. Chem., Int. Ed.* **2013**, *52*, 2166−2179.
(9) Yuyama, H.; Watanabe, T.; Ma, G. H.; Nagai, M.; Omi, S. *Colloids Surf., A* **2000**, *168*, 159−174.
(10) Kobayashi, I.; Mukataka, S.; Nakajima, M. *Ind. Eng. Chem. Res.* **2005**, *44*, 5852−5856.
(11) Allen, K.; Davey, R. J.; Ferrari, E.; Towler, C.; Tiddy, G. J.; Jones, M. O.; Pritchard, R. G. *Cryst. Growth Des.* **2002**, *2*, 523−527.
(12) Yano, J.; Füredi-Milhofer, H.; Wachtel, E.; Garti, N. *Langmuir.* **2000**, *16*, 10005−10014.
(13) Dombrowski, R. D.; Litster, J. D.; Wagner, N. J.; He, Y. *Chem. Eng. Sci.* **2007**, *62*, 4802−4810.
(14) Dombrowski, R. D.; Litster, J. D.; Wagner, N. J.; He, Y. *AIChE J.* **2010**, *56*, 79−91.
(15) Ildefonso, M.; Candoni, N.; Veesler, S. *Org. Process Res. Dev.* **2012**, *16*, 556−560.
(16) Teychené, S.; Biscans, B. *Cryst. Growth Des.* **2011**, *11*, 4810−4818.
(17) Eder, R. J.; Schrank, S.; Besenhard, M. O.; Roblegg, E.; Gruber-Woelfler, H.; Khinast, J. G. *Cryst. Growth Des.* **2012**, *12*, 4733−4738.
(18) Kim, K. J.; Oleksak, R. P.; Hostetler, E. B.; Peterson, D. A.; Chandran, P.; Schut, D. M.; Paul, B. K.; Herman, G. S.; Chang, C. H. *Cryst. Growth Des.* **2014**, *14*, 5349−5355.
(19) Jiang, M.; Zhu, Z.; Jimenez, E.; Papageorgiou, C. D.; Waetzig, J.; Hardy, A.; Langston, M.; Braatz, R. D. *Cryst. Growth Des.* **2014**, *14*, 851−860.
(20) Poulsen, B. J.; Young, E.; Coquilla, V.; Katz, M. *J. Pharm. Sci.* **1968**, *57*, 928−933.
(21) Sloan, K. B.; Koch, S. A.; Siver, K. G.; Flowers, F. P. *J. Invest. Dermatol.* **1986**, *87*, 244−252.
(22) Greenhalgh, D. J.; Williams, A. C.; Timmins, P.; York, P. *J. Pharm. Sci.* **1999**, *88*, 1182−1190.
(23) Barton, A. F. *CRC Handbook of Solubility Parameters and Other Cohesion Parameters*; CRC Press: Boca Raton, FL, 1991; p 278.
(24) Otozai, K.; Tohyama, I. *Fresenius J. Anal. Chem.* **1976**, *281*, 131−133.
(25) Daubert, T. E.; Danner, R. P. *Physical and Thermodynamic Properties of Pure Chemicals: Data Compilation*; Hemisphere: New York, 1989.
(26) Jouyban, A.; Soltanpour, S.; Acree, W. E., Jr. *J. Chem. Eng. Data* **2010**, *55*, 5252−5257.
(27) Grimmett, G.; Stirzaker, D. *Probability and Random Processes*; Clarendon Press: Oxford, 1992; Vol. 2.
(28) Röpke, G.; Priezzhev, V. B. *Nucleation Theory and Applications*; Schmelzer, J. W., Ed.; Wiley-VCH: Weinheim, 2005; pp 77−79.
(29) Butler, B. *Modelling industrial lactose crystallization*. Ph.D. Thesis, University of Queensland, 1998.
(30) Lindenberg, C.; Krättli, M.; Cornel, J.; Mazzotti, M.; Brozio, J. *Cryst. Growth Des.* **2008**, *9*, 1124−1136.
(31) Rashid, M. A. *Crystallization engineering of ibuprofen for pharmaceutical formulation*. Ph.D. Thesis, University of Queensland, 2011.
(32) Husny, J.; Jin, H.; Harvey, E. C.; Cooper-White, J. *Smart Mater. Struct.* **2006**, *15*, S117.
(33) Zheng, B.; Roach, L. S.; Ismagilov, R. F. *J. Am. Chem. Soc.* **2003**, *125*, 11170−11171.
(34) Wang, K.; Lu, Y. C.; Tan, J.; Yang, B. D.; Luo, G. S. *Microfluid. Nanofluid.* **2010**, *8*, 813−821.
(35) Jiang, K.; Lu, A. X.; Dimitrakopoulos, P.; DeVoe, D. L.; Raghavan, S. R. *J. Colloid Interface Sci.* **2015**, *448*, 275−279.
(36) Jiang, S.; ter Horst, J. H. *Cryst. Growth Des.* **2010**, *11*, 256−261.
(37) Lindenberg, C.; Krättli, M.; Cornel, J.; Mazzotti, M.; Brozio. *J. Cryst. Growth Des.* **2008**, *9*, 1124−1136.
(38) Miyasaka, E.; Ebihara, S.; Hirasawa, I. *J. Cryst. Growth.* **2006**, *295*, 97−101.
(39) Hammond, R. B.; Pencheva, K.; Roberts, K. J. *Cryst. Growth Des.* **2006**, *6*, 1324−1334.

DOI: 10.1021/acs.cgd.5b00150
Cryst. Growth Des. 2015, 15, 3645−3651